How to cite: Angew. Chem. Int. Ed. 2024, e202400475
doi.org/10.1002/anie.202400475

Spirobifluorene-Based Porous Organic Salts: Their Porous Network Diversification and Construction of Chiral Helical Luminescent Structures

*Kohei Okubo[+], Kouki Oka[+], Keiho Tsuchiya, Atsunori Tomimoto, and Norimitsu Tohnai**

Abstract: Porous organic salts (POSs) are organic porous materials assembled via charge-assisted hydrogen bonds between strong acids and bases such as sulfonic acids and amines. To diversify the network topology of POSs and extend its functions, this study focused on using 4,4′,4″,4‴-(9,9′-spirobi[fluorene]-2,2′,7,7′-tetrayl)tetrabenzenesulfonic acid (**spiroBPS**), which is a tetrasulfonic acid comprising a square planar skeleton. The POS consisting of **spiroBPS** and triphenylmethylamine (**TPMA**) (**spiroBPS/TPMA**) was constructed from the two-fold interpenetration of an orthogonal network with *pts* topology, which has not been reported in conventional POSs, owing to the shape of the spirobifluorene backbone. Furthermore, combining tris(4-chlorophenyl)methylamine (**TPMA-Cl**) and tris(4-bromophenyl)methylamine (**TPMA-Br**), which are bulkier than **TPMA** owing to the introduction of halogens at the *p*-position of the phenyl groups with **spiroBPS** allows us to construct novel POSs (**spiroBPS/TPMA-Cl** and **spiroBPS/TPMA-Br**). These POSs were constructed from a chiral helical network with *pth* topology, which was induced by the steric hindrance between the halogens and the curved fluorene skeleton. Moreover, **spiroBPS/TPMA-Cl** with ***pth*** topology exhibited circularly polarized luminescence (CPL) in the solid state, which has not been reported in hydrogen-bonded organic frameworks (HOFs).

[*] K. Okubo,[+] K. Oka,[+] K. Tsuchiya, A. Tomimoto, N. Tohnai
Department of Applied Chemistry
Graduate School of Engineering, Osaka University
2-1 Yamadaoka, Suita, Osaka 565-0871, Japan
E-mail: tohnai@chem.eng.osaka-u.ac.jp

K. Oka[+]
Center for Future Innovation (CFi)
Graduate School of Engineering, Osaka University
2-1 Yamadaoka, Suita, Osaka 565-0871, Japan

K. Oka[+]
Institute of Multidisciplinary Research for Advanced Materials,
Tohoku University
2-1-1 Katahira, Aoba-ku, Sendai, Miyagi 980-8577, Japan

[+] K. Okubo and K. Oka contributed equally to this work.

Introduction

Organic-based porous materials, containing organic molecules as building blocks, include metal–organic frameworks (MOFs),[1] which are constructed by coordination bonds, and covalent organic frameworks (COFs),[2] which are constructed by covalent bonds. These materials have been aggressively investigated owing to their high structural designability. Specifically, diversifications in pore shapes, pore environments, and functions have been achieved by modifying the molecular building blocks, and they are expected to be used in a wide range of applications, such as gas storage and separation,[3] heterogeneous catalysis,[4] and sensing.[5]

Recently, a new class of organic-based porous materials, porous organic salts (POSs)[6] has emerged. POSs are a type of hydrogen-bonded organic frameworks (HOFs).[7] Among the many kinds of hydrogen bonds, POSs are mainly constructed by highly ionic hydrogen bonds, that is, charge-assisted hydrogen bonds between strong acids and bases. In charge-assisted hydrogen bonds, the acidity and basicity of the building blocks affect their strength.[6a] Therefore, POSs with charge-assisted hydrogen bonds can be more rigid than HOFs with neutral hydrogen bonds. In addition, POSs are composed of multiple molecules, i.e., acid molecules and base molecules, allowing to achieve various porous structures and functionalities. As with common hydrogen bonds, charge-assisted hydrogen bonds can be reversibly associated and dissociated, thereby allowing **POS**s to form thermodynamically stable and highly crystalline structures. Moreover, their high solubility in polar organic solvents such as methanol, *N*,*N*-dimethylacetamide, *N*, *N*-dimethylformamide, and dimethyl sulfoxide, allows POSs to be dissolved back into the constituting components and to be formed via recrystallization. This would be good for processing the POSs, for instance, into membranes,[8] which is very important for their applications. As shown on the left side of Figure 1a, when bulky **TPMA** derivatives and sulfonic acids were combined, they specifically formed [4+4] supramolecular clusters, these supramolecular clusters self-assemble to form a ***dia*** network (Figure 1a, center). The networks are subsequently interpenetrated to construct diamondoid porous organic salts (*d*-POSs)[6c–f] (Figure 1a, right). The hierarchical construction of *d*-POSs based on the formation of supramolecular clusters suppresses excessive network interpenetration, and results in high porosity.[6d] However, previous studies have used linear or tetrahedral

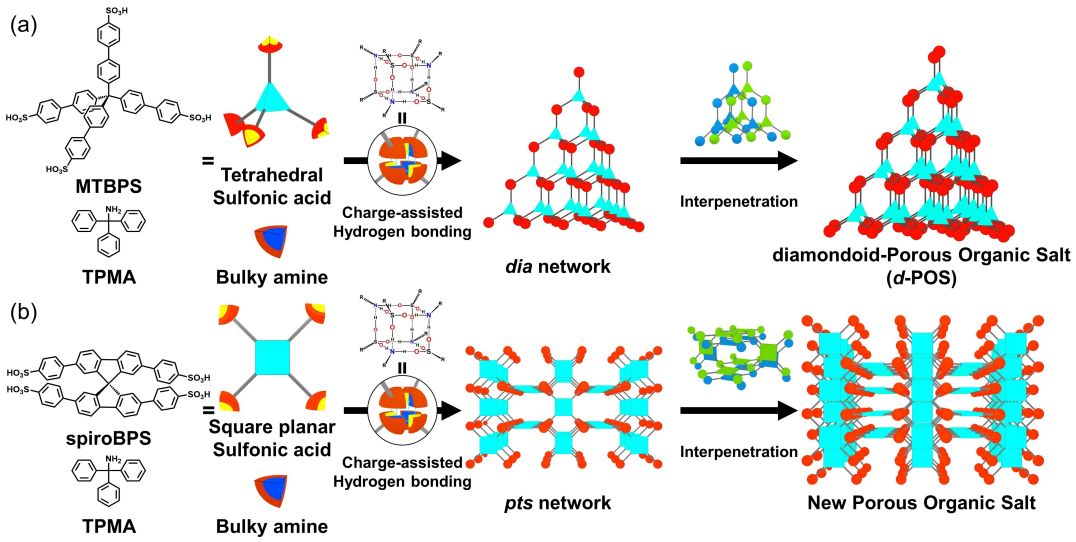

Figure 1. Schematic representations of the construction of POSs using **TPMA** with (a) **MTBPS** or (b) **spiroBPS**.

sulfonic acids because the objective of those studies was to construct stable and rigid HOFs with permanent porosity.[6d–f] Therefore, the topology of the constructed networks was limited to ***dia*** networks owing to the tetrahedral shape of the supramolecular cluster. The topology of the network determines the pore shape and heavily affects the functionality of the porous material, and therefore diversification of topology is very important for the development of POSs.

In this study, we attempted to diversify the network topology of POSs by varying the shape of the molecular skeleton in the building blocks, particularly sulfonic acids. To this purpose, we chose 4,4′,4″,4‴-(9,9′-spirobi[fluorene]-2,2′,7,7′-tetrayl)tetrabenzenesulfonic acid (**spiroBPS**), a rigid and almost square-shaped tetrasulfonic acid comprising of a square planar skeleton (Figure 1b, left) that prevent to form a ***dia*** network.

Results and Discussion

SpiroBPS/TPMA, a porous organic salt, was prepared by mixing **spiroBPS** (i.e., a square-planar tetrasulfonic acid) and **TPMA** at a molar ratio of 1:4 in methanol, followed by recrystallization using mesitylene as a template molecule. The formation of charge-assisted hydrogen bonds between **spiroBPS** and **TPMA** was confirmed by ^{1}H NMR. The protonation of the amino group of **TPMA** resulted in a large downfield shift of its chemical shift, which was attributed to strong deshielding[9] (Figure S1a).

The crystal structure of **spiroBPS/TPMA** was determined by single-crystal X-ray crystallography (Figure 2a, network). In **spiroBPS/TPMA**, **spiroBPS** was arranged in one-dimensional chains and formed an orthogonal network with ***pts*** topology by crossing each other perpendicularly at the supramolecular clusters (Figure 2, charge-assisted hydrogen bonding and Figure S2a). Then, the porous structure was constructed by the two-fold interpenetration of this ***pts*** network (Figure 2a, network). The pores filled with template molecules were micropores, with diameters of 3.6–6.5 Å, had a porosity of 23 %, as calculated by the PLATON/VOID routine[10] (Figure 2a, crystal structure). This pore size was smaller than that of conventional *d*-POSs (4.5–13 Å). The reasons for these results are discussed in the following sections.

Representative porous structures formed by the network with two types of topologies, ***dia*** and ***pts***, are shown in Figures 3a and 3b, respectively. Evidently, the ***dia*** topology, which constructs *d*-POSs, forms green hexagonal windows, whereas the ***pts*** topology, which constructs **spiroBPS/TPMA**, forms small orange square windows and large blue hexagonal windows. For the same edge length, the pore diameters in the decreasing order are as follows: Blue hexagonal, green hexagonal, and orange square windows. The interpenetrated network fills the blue hexagonal windows in **spiroBPS/TPMA**, leaving only the orange square pores, and thereby leading to smaller pores than those reported in previous studies.[6c–f]

Thermogravimetric analysis (**TGA**) shows the high thermal stability of **spiroBPS/TPMA**, with decomposition temperatures exceeding 200 °C (Figure S3a). A template-free **spiroBPS/TPMA** sample was prepared for gas adsorption measurements by removing the template molecules via solvent exchange with diethyl ether followed by thermal activation at 100 °C. PXRD measurements confirmed that **spiroBPS/TPMA** did not show any shift in the peak position before and after activation (Figure S4a, blue and red lines), indicating structural stability that maintained the original structure of the sample after activation. The gas adsorption properties of activated **spiroBPS/TPMA** were evaluated using carbon dioxide (CO_2, 195 K), nitrogen (N_2, 77 K), oxygen (O_2, 77 K), and hydrogen (H_2, 77 K) as shown in Figure 4. The adsorbed amount of gas was 191 mL (STP)/g @0.20 atm for O_2, 147 mL (STP)/g @1.0 atm for N_2, 125 mL (STP)/g @1.0 atm for CO_2, and 77.3 mL (STP)/g @1.0 atm for H_2. The adsorption isotherms for all gases were Type I,

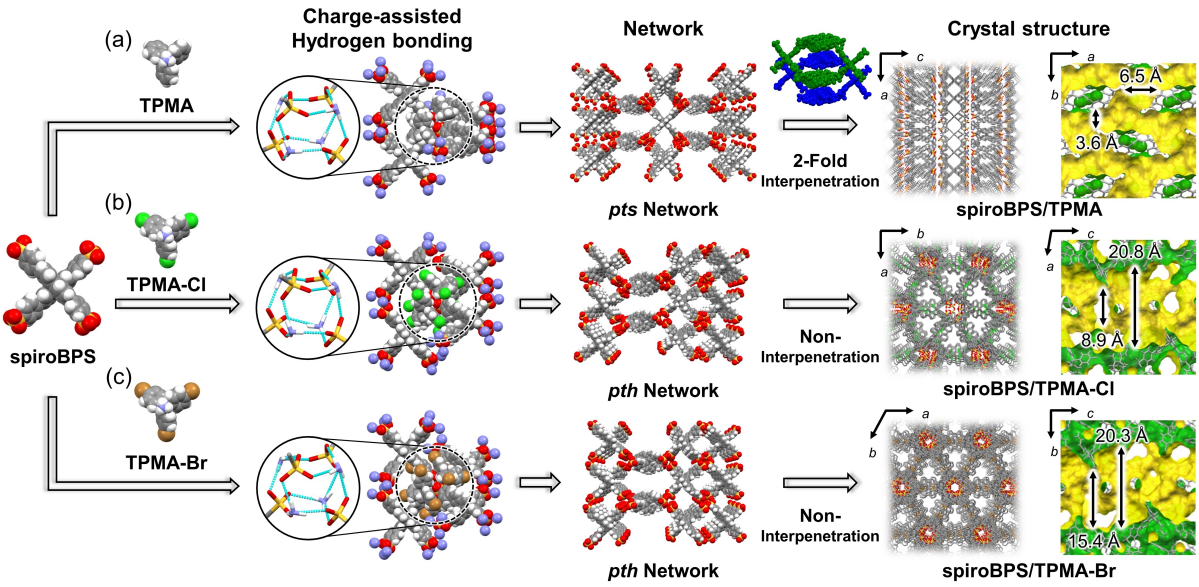

Figure 2. Schematic representations of the construction and the resulting porous and solvent-accessible void structures of (a) **spiroBPS/TPMA**, (b) **spiroBPS/TPMA-Cl**, and (c) **spiroBPS/TPMA-Br**.

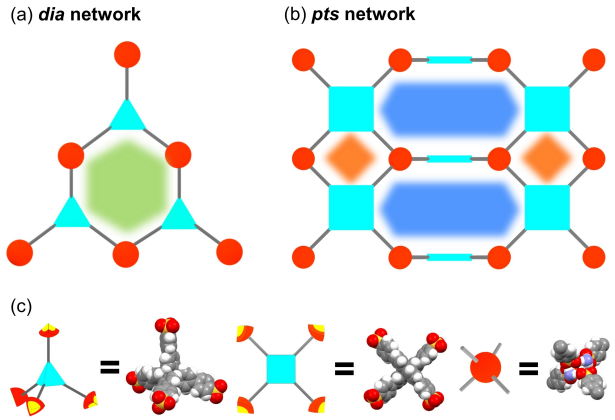

Figure 3. Schematic representations of the pore shapes in the (a) ***dia*** network, (b) ***pts*** network, and (c) their building blocks.

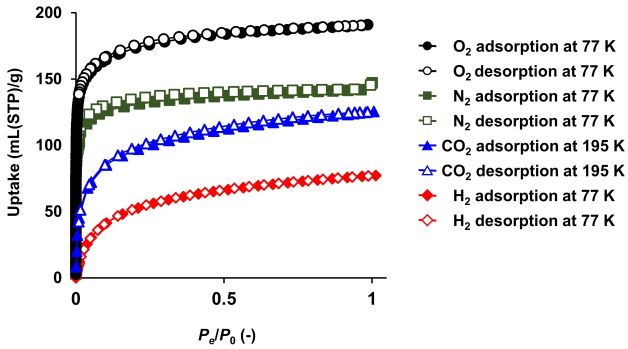

Figure 4. Gas adsorption isotherms of activated **spiroBPS/TPMA** at 195 K for CO_2 and 77 K for O_2, N_2, and H_2.

indicating that the micropores observed in the crystal structure before activation were retained. The Brunauer–Emmett–Teller (BET) surface area calculated from the N_2 adsorption isotherms was 511 m^2/g, showing a larger BET surface area than that of conventional *d*-POSs (439 m^2/g[6f]) despite the lower porosity (23 %) obtained in the present study. Furthermore, conventional *d*-POSs composed of unsubstituted **TPMA**[6c,e,f] had a weak interaction with gas molecules and selectively adsorbed only CO_2, which has a strong quadrupole-quadrupole interaction with aromatic rings.[11] On the other hand, **spiroBPS/TPMA** formed micropores, which had a strong confinement effect[12] on gas molecules and adsorbed a wide range of gases (O_2, N_2, CO_2, H_2). Specifically, O_2 showed a larger amount of adsorption than other gases due to its kinetic diameter which is slightly smaller than the minimum pore diameter of **spiroBPS/TPMA** (3.6 Å).

To further diversify the network topology, **POS**s were prepared by combining **spiroBPS** with **TPMA–X** (**X=Cl**, **Br**), which is halogenated at the *p*-position of **TPMA**. In the crystal structure of **spiroBPS/TPMA**, the distance between hydrogen centers at the *p*-position of **TPMA** between the supramolecular clusters was 3.06 Å (Figure S7). The halogenation of the *p*-position increases the van der Waals radius from 1.22 Å (hydrogen atom) to 1.75 Å (chlorine atom) and 1.85 Å (bromine atom), resulting in steric hindrance by the collision of **TPMA** substituents between the supramolecular clusters, which prevents the formation of the same molecular configuration as **spiroBPS/TPMA**, and is expected to result in the construction of a different network.

Single-crystal X-ray crystallography revealed that **spiroBPS/TPMA–X** was constructed by the non-interpenetration of a helical network with ***pth*** topology (Figure S2b), in which one-dimensional chains formed by **spiroBPS** were crisscrossed at 60° (Figures 2b and 2c). The pores were extended in a three-dimensional network, with a pore size

8.9–20.8 Å and a porosity of 52 % for **spiroBPS/TPMA-Cl** (Figure 2b), and with a pore size 15.4–20.3 Å and a porosity of 52 % for **spiroBPS/TPMA-Br** (Figure 2c). In contrast to **spiroBPS/TPMA**, the position of the template molecules in **spiroBPS/TPMA–X** could not be determined by single-crystal X-ray crystallography due to their severe disorder caused by the expanded pores,[13] and those residual electron densities were removed by the PLATON/SUEEZE routine.[14] The lower number of interpenetrations caused **spiroBPS/TPMA–X** to exhibit a higher porosity than these of **spiroBPS/TPMA** and most conventional porous POSs (41.4 %[6f]) consisting of sulfonic acid and amine. As the porosity increased, the structure became more flexible, and after activation, crystallinity was likely decreased (Figures S4b and S4c, red lines). However, the original crystallinity could be regenerated by the resoaking in the template molecules (Figures S4b and S4c, brown lines).

To clarify the reasons for the different structures of **spiroBPS/TPMA** and **spiroBPS/TPMA–X**, we focused on four **spiroBPS** molecules forming supramolecular clusters and compared their structures. The spirobifluorene skeleton consists of a curved backbone, which allows the POS's network to expand in multiple directions from a tetrahedral supramolecular cluster (Figure S9, bottom). **SpiroBPS/TPMA** exhibits a highly symmetric 90° crossed conformation with "default" ***pts*** topology (Figure S10, top) due to the absence of steric hindrance. It should be noted that the default structure is the expected structure that would be formed when constructing a periodic structure without a steric hindrance.[15] On the other hand, due to the steric hindrance caused by the substitution at the *p*-position of **TPMA**, **spiroBPS/TPMA–X** is not able to take the same conformation as **spiroBPS/TPMA**. Therefore, by lowering the symmetry (Figure S10, bottom), a sufficiently large space around the sulfo group was obtained for the formation of supramolecular clusters. As a result, **spiroBPS/TPMA–X** exhibits a lower symmetric 60° crossed conformation, leading to the formation of a network with ***pth*** topology.

The **spiroBPS/TPMA–X** is chiral to be constructed from the helical network of the ***pth*** topology without inversion and is expected to show circularly polarized luminescence (CPL). However, no CPL signal was observed in the bulk sample of **spiroBPS/TPMA–X** (Figure 5b). The structure was constructed using mesitylene, an achiral template molecule, which was considered to have crystallized as a racemic conglomerate[16] of right- or left-handed crystals by spontaneous resolution. Therefore, we performed a representative experiment to induce chirality in **spiroBPS/TPMA-Cl** using a chiral template molecule as the chiral source.[17] As a result, by recrystallization with *β*-pinene as a template, chiral structures were successfully obtained comprising of a right-handed helix (***P*-spiroBPS/TPMA-Cl**) (Figure 5a, left) from (+)-*β*-pinene and a left-handed helix (***M*-spiroBPS/TPMA-Cl**) (Figure 5a, right) from (−)-*β*-pinene. In addition, the high phase purity of the obtained chiral structures was confirmed by the good agreement between the calculated and experimental **PXRD** patterns (Figure S11). As with achiral **spiroBPS/TPMA-Cl**, the positions of the template molecules in ***P*-/*M*-spiroBPS/TPMA-Cl** could not be determined, therefore their absolute structures were confirmed by their refined Flack parameter-0.009(8) and 0.011(6).

Solid-state CPL measurements yielded nearly symmetrical CPL signals in response to the helical direction of ***P*-spiroBPS/TPMA-Cl** and ***M*-spiroBPS/TPMA-Cl** (Figure 5b). The emission was violet at a wavelength of approximately 385 nm, which corresponded to the maximum emission wavelength of **spiroBPS** (Figure 5c). The quality of the CPL was evaluated using the luminescence dissymmetry factor g_{lum},[18] defined as the following,

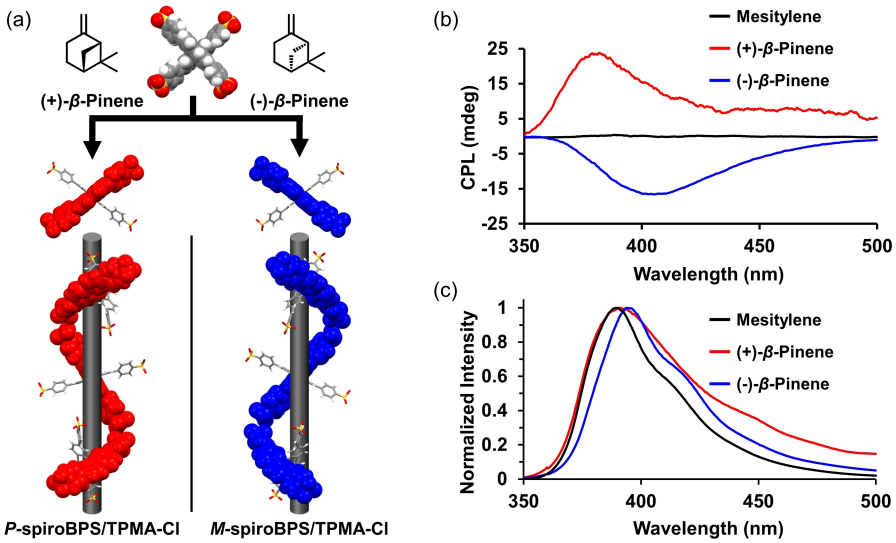

Figure 5. (a) Helical structures, (b) CPL spectra, and (c) PL spectra of **spiroBPS/TPMA-Cl**. In the pre-processing for the measurement, the crystals were gently ground in Fomblin® PFPE (perfluoropolyether) fluid for uniform dispersion. Grinding likely caused partial damage to the crystals, which resulted in low symmetric CPL spectra.[21] In our continuous work, the achievement of membrane fabrication of POSs will eliminate the grinding step in the pre-processing of measurement, and the preparation of a homogeneous membrane will provide high symmetric CPL spectra.

$$g_{lum} = 2\frac{IL - IR}{IL + IR} \quad (1)$$

where I_L and I_R are the intensities of the left- and right-handed CPL, respectively. The maximum calculated g_{lum} values were 4.8×10^{-3} for ***P*-spiroBPS/TPMA-Cl** and -7.0×10^{-3} for ***M*-spiroBPS/TPMA-Cl**, which are comparable to chiral helical polymers ($g_{lum} = 10^{-3}$–10^{-1}).[19] To the best of our knowledge, there is only one study reporting CPL for supramolecular organic frameworks (SOFs)[20], including HOFs, in solution, and no example to date reporting CPL in the solid state. Therefore, **spiroBPS/TPMA-Cl** is the first example of HOF exhibiting CPL in the solid state.

Conclusion

Chirality has been one of the core research topics in the multidisciplinary fields of materials science, chemistry, biology, medicine, and physics. The subject of chirality in materials has recently emerged as a new "growth point" of nanoscience, and major efforts have been made to prepare chiral materials with high chiral purity. In this context, POSs are promising for chiral materials with high chiral purity owing to their high crystallinity resulting from the reversible charge-assisted hydrogen bonds, and their efficient chiral induction from achiral building blocks using chiral solvents and additives can be expected.

In this study, to construct chiral POSs, its network topologies were diversified by utilizing square planar **spiroBPS** and *p*-position modification of **TPMA**–**X**. Depending on the bulkiness of the **TPMA**–**X**, the network topologies of **POS**s were diversified, from an orthogonal network with ***pts*** topology (**spiroBPS/TPMA**), which has not been reported for conventional POSs, to a helical network with ***pth*** topology (**spiroBPS/TPMA-Cl**, **spiroBPS/TPMA-Br**), which is constructed for the first time in all-organic porous materials. Interestingly, the latter structures with ***pth*** topology were chiral even though they consisted of only achiral building blocks, and their right-/left-handed structures were successfully separated by the chiral induction. Furthermore, **spiroBPS/TPMA-Cl** exhibited the first solid-state CPL in HOFs, due to its chiral helical network. In our continuous work, we will investigate the application of POSs, based on the high porosity, chirality, and facile membrane fabrication with the high processability. For example, this application will lead to chiral separation by enantioselective guest adsorption[22] and membrane separation.[23] Therefore, this study shows the proof-of-concept of POSs (one of the HOFs) as chiral materials with high chiral purity owing to their high crystallinity, which accelerates further investigations for chiral materials with high chiral purity.

Acknowledgements

This work was partially supported by Grants-in-Aids for Scientific Research (No. JP20H02548, JP22K14732, JP23K17945, and JP23H03827) from MEXT, Japan. K.Oka. also acknowledges the support from Masuyakinen basic research foundation, Shorai Foundation for Science and Technology, TEPCO Memorial Foundation, Amano Industry Technology Laboratory, Sugiyama Houkoukai, The Yamada Science Foundation, Kenjiro Takayanagi Foundation, Kansai Research Foundation for Technology Promotion, and JACI Prize for Encouraging Young Researcher. K. Okubo. acknowledges the support from JST, the establishment of university fellowships towards the creation of science technology innovation, Grant Number JPMJFS2125. K. Okubo. thanks the Materials Science Research Unit, Osaka University and Honors Program for Graduate Schools in Science, Engineering and Informatics, and the Super Hierarchical Materials Science program in Osaka University.

Conflict of Interest

The authors declare no conflict of interest.

Data Availability Statement

The data that support the findings of this study are available from the corresponding author upon reasonable request.

Keywords: Network topology · Organic salts · Hydrogen bonding · Chiral helical structure · Circularly polarized luminescence

[1] a) J. K. Zaręba, M. Nyk, M. Samoć, *Cryst. Growth Des.* **2016**, *16*, 6419–6425; b) L. D. Tijing, J. R. C. Dizon, I. Ibrahim, A. R. N. Nisay, H. K. Shon, R. C. Advincula, *Applied Materials Today* **2020**, *18*; c) K. Fujii, A. Lazuen Garay, J. Hill, E. Sbircea, Z. Pan, M. Xu, D. C. Apperley, S. L. James, K. D. Harris, *Chem. Commun. (Camb.)* **2010**, *46*, 7572–7574; d) S. Zhou, X. Kong, B. Zheng, F. Huo, M. Stromme, C. Xu, *ACS Nano* **2019**, *13*, 9578–9586; e) Y. Cui, B. Li, H. He, W. Zhou, B. Chen, G. Qian, *Acc. Chem. Res.* **2016**, *49*, 483–493; f) S. Dang, Q.-L. Zhu, Q. Xu, *Nat. Rev. Mater.* **2017**, *3*; g) H. Furukawa, K. E. Cordova, M. O'Keeffe, O. M. Yaghi, *Science* **2013**, *341*, 1230444; h) A. Kirchon, L. Feng, H. F. Drake, E. A. Joseph, H. C. Zhou, *Chem. Soc. Rev.* **2018**, *47*, 8611–8638; i) B. Li, H. M. Wen, Y. Cui, W. Zhou, G. Qian, B. Chen, *Adv. Mater.* **2016**, *28*, 8819–8860; j) H. C. Zhou, S. Kitagawa, *Chem. Soc. Rev.* **2014**, *43*, 5415–5418.

[2] a) A. P. Côté, A. I. Benin, N. W. Ockwig, M. O'Keeffe, A. J. Matzger, O. M. Yaghi, *Science* **2005**, *310*, 1166–1170; b) C. S. Diercks, O. M. Yaghi, *Science* **2017**, *355*; c) K. Geng, T. He, R. Liu, S. Dalapati, K. T. Tan, Z. Li, S. Tao, Y. Gong, Q. Jiang, D. Jiang, *Chem. Rev.* **2020**, *120*, 8814–8933; d) S. Kandambeth, K. Dey, R. Banerjee, *J. Am. Chem. Soc.* **2019**, *141*, 1807–1822.

[3] a) H. Li, K. Wang, Y. Sun, C. T. Lollar, J. Li, H.-C. Zhou, *Mater. Today* **2018**, *21*, 108–121; b) Z. Wang, S. Zhang, Y. Chen, Z. Zhang, S. Ma, *Chem. Soc. Rev.* **2020**, *49*, 708–735; c) S. Yuan, X. Li, J. Zhu, G. Zhang, P. Van Puyvelde, B. Van der Bruggen, *Chem. Soc. Rev.* **2019**, *48*, 2665–2681; d) X. Zhao, Y. Wang, D. S. Li, X. Bu, P. Feng, *Adv. Mater.* **2018**, *30*, e1705189.

[4] a) A. Dhakshinamoorthy, Z. Li, H. Garcia, *Chem. Soc. Rev.* **2018**, *47*, 8134–8172; b) C. Y. Lin, D. Zhang, Z. Zhao, Z. Xia, *Adv. Mater.* **2018**, *30*; c) J. Liu, L. Chen, H. Cui, J. Zhang, L. Zhang, C. Y. Su, *Chem. Soc. Rev.* **2014**, *43*, 6011–6061; d) S. M. J. Rogge, A. Bavykina, J. Hajek, H. Garcia, A. I. Olivos-Suarez, A. Sepulveda-Escribano, A. Vimont, G. Clet, P. Bazin, F. Kapteijn, M. Daturi, E. V. Ramos-Fernandez, I. X. F. X. Llabres, V. Van Speybroeck, J. Gascon, *Chem. Soc. Rev.* **2017**, *46*, 3134–3184.

[5] a) X. Liu, D. Huang, C. Lai, G. Zeng, L. Qin, H. Wang, H. Yi, B. Li, S. Liu, M. Zhang, R. Deng, Y. Fu, L. Li, W. Xue, S. Chen, *Chem. Soc. Rev.* **2019**, *48*, 5266–5302; b) W. P. Lustig, S. Mukherjee, N. D. Rudd, A. V. Desai, J. Li, S. K. Ghosh, *Chem. Soc. Rev.* **2017**, *46*, 3242–3285; c) Y. Zhang, S. Yuan, G. Day, X. Wang, X. Yang, H.-C. Zhou, *Coord. Chem. Rev.* **2018**, *354*, 28–45.

[6] a) G. Xing, T. Yan, S. Das, T. Ben, S. Qiu, *Angew. Chem. Int. Ed. Engl.* **2018**, *57*, 5345–5349; b) G. Xing, I. Bassanetti, S. Bracco, M. Negroni, C. Bezuidenhout, T. Ben, P. Sozzani, A. Comotti, *Chem. Sci.* **2019**, *10*, 730–736; c) A. Yamamoto, T. Hasegawa, T. Hamada, T. Hirukawa, I. Hisaki, M. Miyata, N. Tohnai, *Chemistry* **2013**, *19*, 3006–3016; d) A. Yamamoto, S. Uehara, T. Hamada, M. Miyata, I. Hisaki, N. Tohnai, *Cryst. Growth Des.* **2012**, *12*, 4600–4606; e) A. Yamamoto, T. Hirukawa, I. Hisaki, M. Miyata, N. Tohnai, *Tetrahedron Lett.* **2013**, *54*, 1268–1273; f) T. Ami, K. Oka, K. Tsuchiya, N. Tohnai, *Angew. Chem. Int. Ed. Engl.* **2022**, *61*, e202202597.

[7] a) I. Hisaki, C. Xin, K. Takahashi, T. Nakamura, *Angew. Chem. Int. Ed. Engl.* **2019**, *58*, 11160–11170; b) B. Wang, R. B. Lin, Z. Zhang, S. Xiang, B. Chen, *J. Am. Chem. Soc.* **2020**, *142*, 14399–14416; c) R. B. Lin, Y. He, P. Li, H. Wang, W. Zhou, B. Chen, *Chem. Soc. Rev.* **2019**, *48*, 1362–1389; d) Y. Zou, W. Cui, D. Chen, F. Luo, H. Li, *ACS Appl. Mater. Interfaces* **2023**, *15*, 47463–47474.

[8] T. Hosokawa, S. Inazato, A. Yamamoto, N. Tohnai, *Mater. Lett.* **2022**, *327*, 133054.

[9] E. Arunan, G. R. Desiraju, R. A. Klein, J. Sadlej, S. Scheiner, I. Alkorta, D. C. Clary, R. H. Crabtree, J. J. Dannenberg, P. Hobza, H. G. Kjaergaard, A. C. Legon, B. Mennucci, D. J. Nesbitt, *Pure Appl. Chem.* **2011**, *83*, 1619–1636.

[10] A. L. Spek, *Acta Crystallogr. Sect. D* **2009**, *65*, 148–155.

[11] a) J. H. Williams, *Acc. Chem. Res.* **1993**, *26*, 593–598; b) M. R. Battaglia, A. D. Buckingham, J. H. Williams, *Chem. Phys. Lett.* **1981**, *78*, 421–423; c) J. R. Li, R. J. Kuppler, H. C. Zhou, *Chem. Soc. Rev.* **2009**, *38*, 1477–1504.

[12] a) K. Adil, Y. Belmabkhout, R. S. Pillai, A. Cadiau, P. M. Bhatt, A. H. Assen, G. Maurin, M. Eddaoudi, *Chem. Soc. Rev.* **2017**, *46*, 3402–3430; b) D. Lin, S. Tu, L. Yu, Y. Yuan, Y. Wu, X. Zhou, Z. Li, Q. Xia, *Ind. Eng. Chem. Res.* **2023**, *62*, 5252–5261; c) L. Hu, W. Wu, L. Gong, H. Zhu, L. Jiang, M. Hu, D. Lin, K. Yang, *Angew. Chem. Int. Ed. Engl.* **2023**, *62*, e202215296; d) M. Chang, T. Yan, Y. Wei, J. X. Wang, D. Liu, J. F. Chen, *ACS Appl. Mater. Interfaces* **2022**, *14*, 25374–25384.

[13] X. G. Liu, H. Wang, B. Chen, Y. Zou, Z. G. Gu, Z. Zhao, L. Shen, *Chem. Commun. (Camb.)* **2015**, *51*, 1677–1680.

[14] A. L. Spek, *Acta Crystallogr C Struct Chem* **2015**, *71*, 9–18.

[15] a) O. M. Yaghi, M. O'Keeffe, N. W. Ockwig, H. K. Chae, M. Eddaoudi, J. Kim, *Nature* **2003**, *423*, 705–714; b) M. Li, D. Li, M. O'Keeffe, O. M. Yaghi, *Chem. Rev.* **2014**, *114*, 1343–1370.

[16] L. Perez-Garcia, D. B. Amabilino, *Chem. Soc. Rev.* **2007**, *36*, 941–967.

[17] Y. Lu, H. Zhang, Y. Zhu, P. J. Marriott, H. Wang, *Adv. Funct. Mater.* **2021**, *31*.

[18] R. Carr, N. H. Evans, D. Parker, *Chem. Soc. Rev.* **2012**, *41*, 7673–7686.

[19] E. M. Sanchez-Carnerero, A. R. Agarrabeitia, F. Moreno, B. L. Maroto, G. Muller, M. J. Ortiz, S. de la Moya, *Chemistry* **2015**, *21*, 13488–13500.

[20] Y. Li, Q. Li, X. Miao, C. Qin, D. Chu, L. Cao, *Angew. Chem. Int. Ed. Engl.* **2021**, *60*, 6744–6751.

[21] M. Louis, R. Sethy, J. Kumar, S. Katao, R. Guillot, T. Nakashima, C. Allain, T. Kawai, R. Metivier, *Chem. Sci.* **2019**, *10*, 843–847.

[22] a) J. Navarro-Sanchez, A. I. Argente-Garcia, Y. Moliner-Martinez, D. Roca-Sanjuan, D. Antypov, P. Campins-Falco, M. J. Rosseinsky, C. Marti-Gastaldo, *J. Am. Chem. Soc.* **2017**, *139*, 4294–4297; b) Y. Peng, T. Gong, Y. Cui, *Chem. Commun. (Camb.)* **2013**, *49*, 8253–8255.

[23] a) Z. Kang, M. Xue, L. Fan, J. Ding, L. Guo, L. Gao, S. Qiu, *Chem. Commun. (Camb.)* **2013**, *49*, 10569–10571; b) J. Y. Chan, H. Zhang, Y. Nolvachai, Y. Hu, H. Zhu, M. Forsyth, Q. Gu, D. E. Hoke, X. Zhang, P. J. Marriot, H. Wang, *Angew. Chem. Int. Ed. Engl.* **2018**, *57*, 17130–17134.

Manuscript received: January 8, 2024
Accepted manuscript online: January 27, 2024
Version of record online: ■■, ■■

Research Articles

K. Okubo, K. Oka, K. Tsuchiya, A. Tomimoto, N. Tohnai* — **e202400475**

Spirobifluorene-Based Porous Organic Salts: Their Porous Network Diversification and Construction of Chiral Helical Luminescent Structures

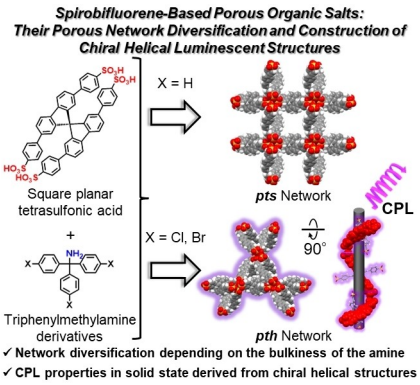

Porous organic salts (POSs) with a chiral helical network were constructed from a square-planar sulfonic acid and *p*-position-modified triphenylmethylamine, both achiral components. The chirality of the POSs could be controlled by chiral induction, and the obtained porous materials composed of hydrogen bonds exhibited solid-state circularly polarized luminescence (CPL). This study highlights applications for POSs as chiral materials.